Review of Scientific Instruments

Heat diffusion imaging: In-plane thermal conductivity measurement of thin films in a broad temperature range

Cite as: Rev. Sci. Instrum. **91**, 113701 (2020); https://doi.org/10.1063/5.0024476
Submitted: 07 August 2020 . Accepted: 10 October 2020 . Published Online: 02 November 2020

Tianhui Zhu, David H. Olson, Patrick E. Hopkins, and Mona Zebarjadi

Review of Scientific Instruments ARTICLE scitation.org/journal/rsi

Heat diffusion imaging: In-plane thermal conductivity measurement of thin films in a broad temperature range

Cite as: Rev. Sci. Instrum. 91, 113701 (2020); doi: 10.1063/5.0024476
Submitted: 7 August 2020 • Accepted: 10 October 2020 •
Published Online: 2 November 2020

Tianhui Zhu,[1] David H. Olson,[2] Patrick E. Hopkins,[2,3,4] and Mona Zebarjadi[1,3,a)]

AFFILIATIONS

[1]Department of Electrical and Computer Engineering, University of Virginia, Charlottesville, Virginia 22904, USA
[2]Department of Mechanical and Aerospace Engineering, University of Virginia, Charlottesville, Virginia 22904, USA
[3]Department of Materials Science and Engineering, University of Virginia, Charlottesville, Virginia 22904, USA
[4]Department of Physics, University of Virginia, Charlottesville, Virginia 22904, USA

[a)]**Author to whom correspondence should be addressed:** m.zebarjadi@virginia.edu

ABSTRACT

This work combines the principles of the heat spreader method and the imaging capability of the thermoreflectance measurements to measure the in-plane thermal conductivity of thin films without the requirement of film suspension or multiple thermometer deposition. We refer to this hybrid technique as *heat diffusion imaging*. The thermoreflectance imaging system provides a temperature distribution map across the film surface. The in-plane thermal conductivity can be extracted from the temperature decay profile. By coupling the system with a cryostat, we were able to conduct measurements from 40 K to 400 K. Silicon thin film samples with and without periodic holes were measured and compared with in-plane time-domain thermoreflectance measurements and literature data as validation for heat diffusion imaging.

I. INTRODUCTION

The continuous miniaturization of the electronic and optoelectronic devices results in increased energy dissipation densities and large local temperatures, which compromises the reliable operation of the electronics[1] and calls for small scale thermal management solutions. Thin films are often used in integrated circuits, such as transistors and diodes;[2] in energy conversion technologies, such as light-emitting diodes (LEDs) and solar cells;[3] and as optical, electrical, thermal, or protective coating layers.[4,5] Understanding heat transport in thin films is essential to address microscale to nanoscale heat management and energy conversion and requires accurate measurement of thermal conductivity, which can be challenging in practice.

Measuring the in-plane thermal conductivity of thin film samples often requires film suspension[6–8] and is demanding in terms of the micro-fabrication processes needed. For delicate thin films, it is preferred to measure directly on the substrate and avoid potential damage to the sample during the substrate removal process. In the case of thin films supported on a substrate, which is typical in devices, the options are limited. If the samples are isotropic, a cross-plane measurement can be taken instead, using the 3ω method[9] or the time-domain thermoreflectance (TDTR) method.[10] In the case of anisotropic samples, two established in-plane measurement techniques are the variable-linewidth 3ω method[11,12] and the heat spreader method.[13,14] The variable-linewidth 3ω method requires the knowledge of the cross-plane thermal conductivity value to derive the in-plane one. It needs narrow lines and is limited in the range of measurable thermal conductivity values. When the variable-linewidth 3ω method cannot be applied, the heat spreader method is useful. Both methods use metallic thermometers, and hence, an insulating layer needs to be deposited on conductive samples to prevent current leaks, which can be difficult to implement and reduces the accuracy since the temperature is no longer monitored directly on the sample. There has been an attempt to combine thermoreflectance imaging with finite element modeling for

measurement of the in-plane thermal conductivity of Si thin films at room temperature,[15] but it requires intensive modeling and is considered an indirect method to extract thermal conductivity. Similar combinations of thermoreflectance imaging and finite element modeling have been used by many groups to study heat transport in devices and extract various parameters, such as thermal boundary resistance between the layers and thermal conductivity of each layer of the device.[16–20] While additional opportunities for measuring in-plane thermal conductivities can be provided using TDTR, typical measurements of the technique are utilized for the extraction of the cross-plane thermal conductivity of a material.

Here, we propose an approach that combines thermoreflectance (TR) imaging and the heat spreader method for characterizing the in-plane thermal conductivity of thin films on the substrate, and we refer to this method as heat diffusion imaging. A heater is deposited at one end of the film and subsequently Joule heated. When heat flow reaches the thin film of interest, the film, supported by a low thermal conductivity substrate, spreads the heat laterally. Therefore, it is possible to extract its in-plane thermal conductivity by measuring the temperature decay profile along the film. This is known as the heat spreader method. The traditional heat spreader method requires patterning of a series of metallic lines along the sample. These metallic lines are used as resistance thermometers (thermistors) to detect the local temperatures. To measure temperature, one needs to pass current and measure resistance of the thermistors; hence, deposition of an insulating layer between a conductive sample and these thermistors is needed to avoid a current leak. This indicates that a limited number of data points (equal to the number of thermistors deposited) are available for thermal conductivity extraction, and inaccuracy exists because the temperature is not measured directly on the sample.

With a TR imaging system, the thermistor fabrication processes are no longer necessary. The temperature can be measured directly on the sample and continuously along the film with a spatial resolution on the order of 100 nm. A temperature map of the sample surface is acquired based on how surface reflectivity changes with respect to temperature variations. With heat diffusion imaging, one only needs a metallic heater line deposited on top of the thin film to provide the initial heat flow by Joule heating. The accuracy is improved from the heat spreader method since more temperature-position data points are available for analysis. Heat diffusion imaging is less sensitive to the thermal contact resistance between the thin film sample and the substrate, compared with the 3ω method. It provides a wider range of measurable thermal conductivity compared with in-plane TDTR—as long as the thin film is more conductive compared with the underlying substrate insulating layer, the film's in-plane thermal conductivity can be measured.

Heat diffusion imaging is of interest to the thermal community and in particular of interest to the thermoelectric community. The electrode configuration that is commonly used for thermoelectric power factor measurements can also be used for heat diffusion imaging to enable thermal conductivity measurements and hence extraction of the thermoelectric figure of merit, ZT.

We select silicon thin films as the test bed for our heat diffusion imaging technique, since Si is one of the most studied materials and can serve as a good reference. We measure two samples: one is a plain Si thin film and the other is a holey Si thin film with periodic holes spaced 100 nm apart. Both films are 100 nm thick. The in-plane thermal conductivity of the holey Si sample is greatly reduced compared to that of the in-plane silicon film, as phonons with mean free paths longer than the neck size are suppressed.[21–25] Information on this reduction in thermal conductivity can shed light on the phonon interactions with boundaries and can be useful in finding low thermal conductivity films and, in particular, efficient thermoelectric materials.[23–25] Our measurement results are compared with those measured by in-plane TDTR on the same samples, as well as data from the literature.

II. DEVICE AND METHOD

A. Silicon thin films

An illustration of the device configuration of the two silicon thin film samples is shown in Fig. 1. These devices are fabricated from a silicon on insulator (SOI) wafer and have a 100 nm thick active Si layer of area $30 \times 200\ \mu m^2$, sitting on a 2 μm thick buried oxide (BOX). The holey Si device is boron-doped (3×10^{19} cm^{-3} -10×10^{19} cm^{-3}). The arrays of holes of 55 nm diameter are spaced with a center-to-center distance of 100 nm or, in other words, a neck size of 45 nm. The plain Si thin film is lightly doped (boron, $\sim 10^{16}$ cm^{-3}) and has the same dimensions as the holey silicon film but without the holes. The Al/Au contact (1 μm/50 nm) deposited at the end of the thin film is used as the heater for our measurements, and its length is more than 2500 μm.

B. Heat diffusion imaging

A thermoreflectance imaging system utilizes the fact that the surface reflectivity (R) of a material changes with temperature (T). Their relation is expressed as $\Delta T = \frac{1}{C_{TR}} \frac{\Delta R}{R}$, where C_{TR} is the thermoreflectance coefficient. C_{TR} mainly depends on the material surface, the ambient temperature, and the wavelength of the illumination. In order to find the absolute temperature on the sample surface, C_{TR} has to be known, and it can be calibrated for with controlled temperature changes.

A working diagram of our TR imaging system from Microsanj, LLC,[26] is shown in Fig. 2(a). The function generator generates a

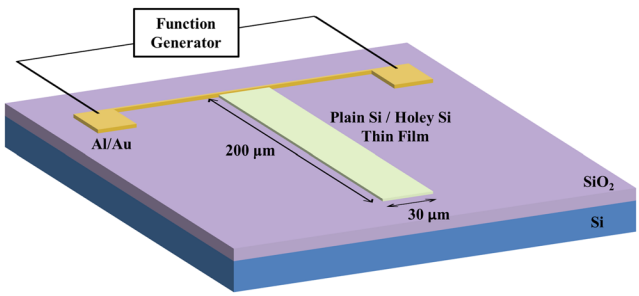

FIG. 1. Schematic drawing of the device configuration. The Al/Au heater is more than 2500 μm in length. The dimensions are not to scale in this drawing.

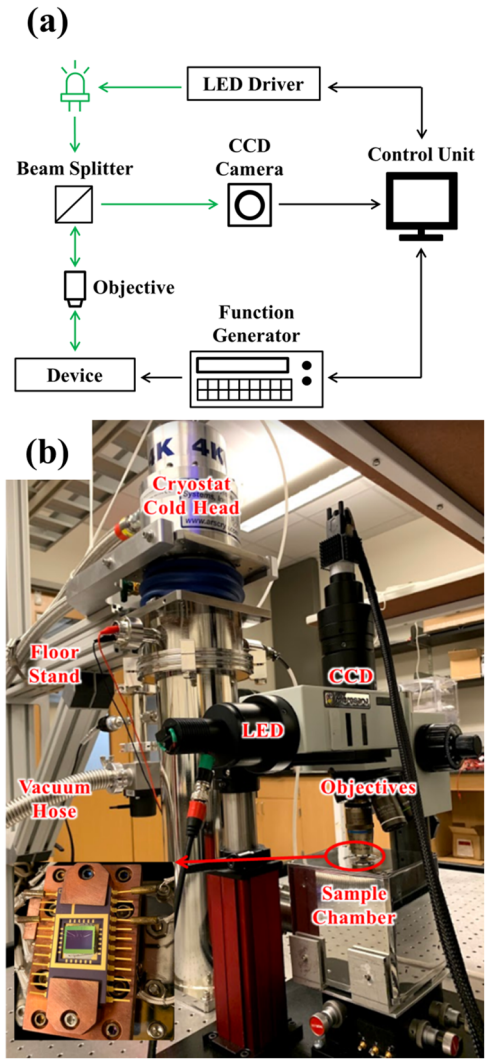

FIG. 2. (a) Working principle of the thermoreflectance imaging system. (b) Picture of the system coupled with a cryostat. The inset shows how a sample is mounted to a DIP and then to the sample stage inside of the sample chamber.

voltage pulse to excite the device under study, which is synchronized with a light pulse emitted from the LED light source (530 nm green light in this case) by the control unit. A charge-coupled device (CCD) camera captures the changes in the reflected light off the sample when the LED is activated and deactivated to determine the temperature change, ΔT, at a certain delay time. The captured reflectivity information is averaged over many thermal excitation cycles to provide a complete temperature map of the area of interest with minimum noise. The magnification of the microscope objective can be selected based on the sample size. The optical resolution of a temperature map is diffraction-limited. For our wavelength of 530 nm, it is about 330 nm under a 100× magnification objective and about 380 nm under 60× magnification.

The in-plane thermal conductivity can be extracted by analyzing how heat propagates along the thin films. When current passes though the metallic line at one end of the Si thin film, the generated heat from Joule heating results in a temperature gradient, which gradually decays with increasing distance away from the heater line. This temperature decay can be described by the classical fin equation[27] and is expected to be exponential in the lateral direction. Temperature, T, as a function of distance away from the heater, x, is

$$T(x) - T(\infty) \propto e^{-\sqrt{h_i/(k_x d)}x} = e^{-\beta x}, \tag{1}$$

where the parameter $\beta = \sqrt{h_i/(k_x d)}$ is defined for simplicity, h_i is the cross-plane thermal conductance of the underlying insulating layer, k_x is the in-plane thermal conductivity of the thin film of interest, and d is its thickness. Dividing the cross-plane thermal conductivity of the substrate insulator, $k_{i,z}$, by the layer thickness, d_i, gives us h_i, i.e., $h_i = k_{i,z}/d_i$. k_x can be extracted from the temperature profile as long as the thin film thickness and the substrate insulating layer parameters are known. This theoretical model has been discussed extensively in the heat spreader method[14] and has been verified for Si thin films on the SiO_2/Si substrate[28] and for few layer graphene on SiO_2.[13]

Since heat diffusion imaging is based on the heat spreader method, similar limitations apply. The thin film of interest should have a large in-plane thermal conductance relative to the cross-plane thermal conductance of the substrate insulating layer. In order to satisfy the conditions of the fin equation, it has been proposed that the healing length, defined as $\beta^{-1} = \sqrt{k_x d d_i/k_{i,z}}$, should be much larger than the combined thickness of the thin film and the substrate insulating layer, $d + d_i$.[28] Jang *et al.* studied heat transfer in a few layers of graphene on SiO_2. Even though the healing length was on the same order of magnitude as the SiO_2 substrate thickness, they have shown that the heat spreader model is still valid,[13] which should be the limiting condition to justify the application of this model. The bulk substrate at the bottom needs to be highly thermally conductive to maintain the isothermal condition.

Figure 2(b) shows the entire setup. The cryostat from Advanced Research Systems (ARS) has been specially engineered so that the sample chamber has an optical window on top for imaging. The window is made of 1 mm thick N-BK7 glass with Vis 0° anti-reflective coating from Edmund Optics, which provides >99.5% transmissivity for wavelength between 425 nm and 675 nm and has a transformation temperature above 800 K. The thickness of the window glass needs to be corrected for by the correction collar of the objective, in order to avoid blurry images caused by changes in the refractive index. We use the 60× magnification objective from Nikon, which can correct for cover glass thickness up to 1.3 mm and offers a relatively long working distance up to 2.6 mm. The sample is wire-bonded to a ceramic dual in-line package (DIP) for electrical connections inside the chamber and is shown in the inset of Fig. 2(b). A heater is embedded in the sample stage to set the temperature. Vibrations caused by the vacuum pump and the helium compressor have been minimized by using low-vibration design from ARS, placing the setup on an optical table, and having a floor stand and sandbags to support the cold head and a stand to support the TR imaging camera system.

C. In-plane time-domain thermoreflectance

We deposit a nominally 80 nm thick Al film on an identical plain Si device for the implementation of time-domain thermoreflectance (TDTR) to extract its in-plane thermal conductivity. We implement a two-tint TDTR configuration, whereby the output of a 80 MHz oscillator centered at 808.5 nm is spectrally separated into pump and probe paths. The pump path is electro-optically modulated and creates a frequency dependent heating event at the sample surface. The probe is mechanically delayed in time and monitors the thermoreflectance at the sample surface, creating a cooling curve that is compared to the heat diffusion equation. Additional details regarding the two-tint experimental configuration,[29] as well as the analyses associated with TDTR,[10,30,31] can be found in the literature. We mount the specimen into a liquid helium cryostat (JANIS ST-100) for measurements at 80 K, 124 K, 193 K, and 294 K.

For the determination of the in-plane thermal conductivity of the Si membrane, we perform measurements in two configurations, following the guidelines of Jiang *et al.*[32] First, we perform TDTR measurements using a 10× objective (effective $1/e^2$ pump/probe radius = 12.3 μm) and moderately high modulation frequencies (8.4 MHz) on the Al/SiO_2 region of the device. This allows us to extract the thermal conductivity of the oxide layer while being negligibly sensitive to the in-plane thermal conductivity of the Al transducer. Next, we perform measurements using a 20× objective (effective $1/e^2$ pump/probe radius = 6.5 μm) and low modulation frequencies (500 kHz) on the Al/SiO_2 region of the device for the extraction of the in-plane thermal conductivity of the Al transducer while fixing the thermal conductivity of the underlying SiO_2. Finally, measurements in this configuration are performed on the Al/Si/SiO_2 stack for the determination of the in-plane thermal conductivity of the Si membrane, where we input the Al and SiO_2 thermal conductivities as known parameters derived from measurements on the Al/SiO_2 region of the device. For all measurements, we assume literature values for the volumetric heat capacities of Al, SiO2, and Si.[33] The error in the reported TDTR values includes uncertainties of 2.5% in the volumetric heat capacities of the Al transducer, Si membrane, and SiO_2 layer, as well as variations in the extracted Al thermal conductivity, typically on the order of 15%–20%. We are not aware of any works examining the spot size dependence of the thermal conductivity of thin Si films measured via TDTR. We note that Wilson and Cahill[34] have examined the spot size dependence of the thermal conductivity of bulk Si. They observed a minimal dependence at spot sizes comparable to those used in this work, and thus, we do not expect our used spot sizes to influence the apparent thermal conductivity of the thin Si film.

III. RESULTS AND DISCUSSION

Pulses of 5 ms duration, up to 5 V and 20% duty cycle, were applied to the heater line at one end of the thin film to generate Joule heating. An example of the temperature decay map of the plain Si thin film in the steady state, averaged over a few hundred thermal excitation cycles and taken under 100× magnification, is shown in Fig. 3(a). A representative map of the holey Si sample is provided by its side in Fig. 3(c) for comparison. The same thermoreflectance coefficient, C_{TR}, is used for all temperature maps across all materials, which means that an arbitrary unit is adopted for temperature. Calibrating for C_{TR} to get the absolute temperatures on the thin films is not necessary here because the parameter β is determined by an exponential fit of the temperature profile and depends only on how fast the temperature drops. Nevertheless, since C_{TR} of Au for our green light wavelength is known,[35] the temperature rise of the heater (less than 50 K) was closely monitored throughout measurements to ensure that it is reasonable to assume a single thermoreflectance coefficient. We have included uncertainties in the sample temperature to account for the impact from this temperature rise. The distance that the temperature gradient extends over is much shorter on the holey Si thin film than on the plain Si one because of a greatly suppressed thermal conductivity.

Knowing that the Si thin film thickness d = 100 nm and that the insulating SiO_2 layer thickness d_i = 2 μm, the in-plane thermal conductivity calculation is reduced to

$$k_x = \frac{h_i}{\beta^2 d} = 5 \times 10^{12} \times \frac{k_{i,z}}{\beta^2}. \quad (2)$$

We use the recommended values of fused SiO_2[36] for $k_{i,z}$ in our calculations, as it has been shown that the temperature dependence of the thermal conductivity of micrometer-thick SiO_2 matches well with the bulk values.[28] h_i is typically on the order of 10^5 W/(m^2 K) –10^6 W/(m^2 K), which means that the air convection to the surroundings[27] and the thermal contact resistance between the Si layer and the SiO_2 layer[37–39] are negligible in comparison. An exponential fit to the temperature line profile taken along the thin film yields β, and then k_x is obtained. A few representative temperature profiles of both films and their corresponding exponential fitting curves at room temperature are shown in Figs. 3(b) and 3(d). As expected, β is smaller for plain Si based on a more gradual temperature decay, which results in a larger k_x. In order to reduce the uncertainty, for each measurement, multiple temperature line profiles that start from the edge of the heater and continue along the length of the thin films have been taken into account and an averaged thermal conductivity is reported.

Temperature dependent data were acquired by repeating the measurements at different sample stage temperatures. The highest magnification offered for an objective with the correction collar and adequate working distance is 60×, so the temperature map resolution is slightly reduced at temperatures other than room temperature. Limited by the working distance of this microscope objective, the mounted sample had to be brought to within 1 mm of the optical window. This led to a discrepancy between the sample stage temperature and the sample surface temperature. This temperature difference was measured using a silicon diode temperature sensor inside the cryostat, by mounting the sensor onto the DIP, where the sample was mounted. The error in the measured sample temperature is estimated to be within 1 K and has been taken into account in the thermal conductivity calculation.

The temperature dependence of the in-plane thermal conductivity of the plain Si film is plotted in Fig. 4 and is compared with data from the literature.[23,40] Phonon-boundary scattering dominates phonon-impurity scattering in micrometer-thick plain Si thin films

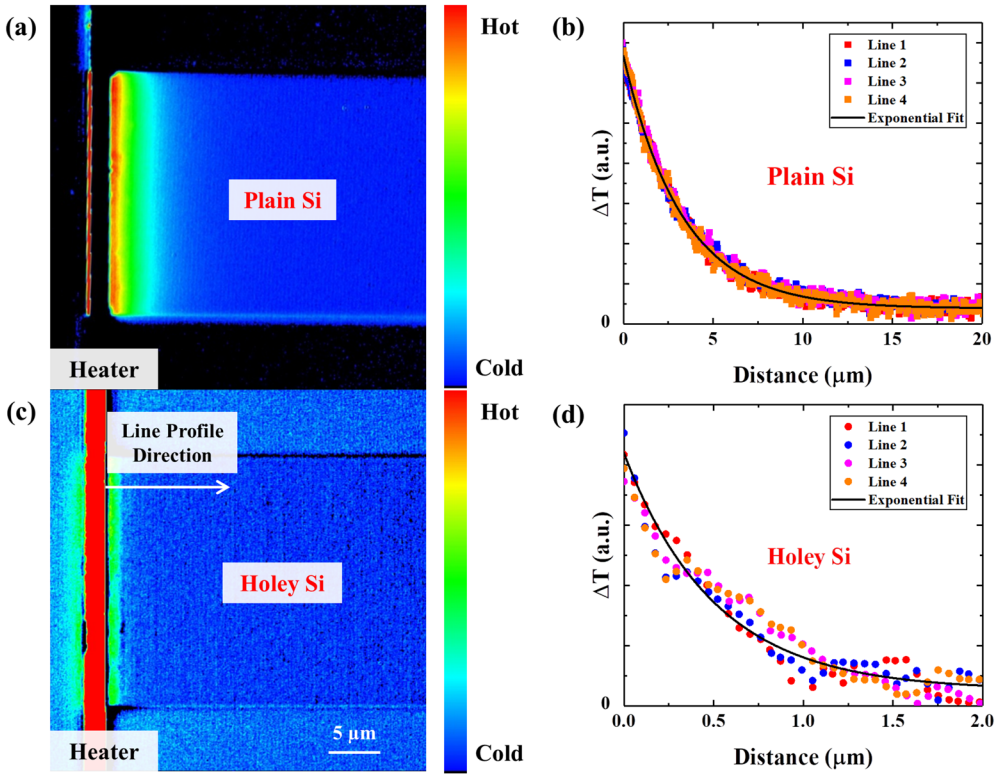

FIG. 3. Example temperature maps of (a) the plain Si sample and (c) the holey Si sample under 100× magnification at room temperature. The same value of thermoreflectance coefficient is assumed for both maps, and an arbitrary unit for temperature is adopted. Note that the heater in (a) is shown in dark color as its thermoreflectance coefficient has an opposite sign to the coefficient assumed; we have chosen the sign of the thermoreflectance coefficient to show information on the thin film. Typically, more than ten temperature line profiles are taken from each temperature map for averaging. A few representative temperature decay curves and their corresponding exponential fitting curves are shown for (b) the plain Si and (d) the holey Si thin films.

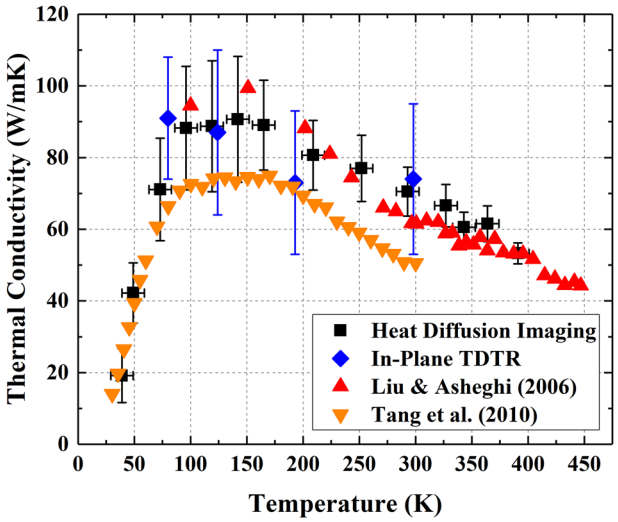

FIG. 4. Temperature dependence of the in-plane thermal conductivity of the plain Si thin film measured by heat diffusion imaging, compared with in-plane TDTR measurement on the same sample and data from the literature on suspended samples of the same thickness (100 nm).[23,40]

with carrier concentration less than 10^{17} cm^{-3}, and their thermal conductivities are nearly identical against temperature, independent of the exact concentrations.[7] Therefore, it is justifiable to compare the results of our 100 nm thick, slightly doped (10^{16} cm^{-3}) plain Si thin film with thermal conductivities of intrinsic silicon thin films of the same thickness.[23,40] Our values agree with literature data for suspended samples in the temperature range from 40 K to 400 K with reasonable errors. While the uncertainty in our TDTR measurements is large, there is generally good agreement found with values extracted from heat diffusion imaging. These comparisons show the feasibility and reliability of the heat diffusion imaging method.

Data for the holey Si sample are presented in Fig. 5. The values are much lower than those of the plain Si sample, as the higher doping concentrations and the periodic holes introduce more frequent phonon scattering events. We were not able to perform TDTR measurements on the in-plane thermal conductivity of the holey Si film due to its low thermal conductivity. As the neck size between holes is the major deciding factor in the suppression of the in-plane thermal conductivity,[21–25] we compared our results with those of suspended holey Si samples of the same thickness but different neck sizes.[23,24] Our values for 45 nm neck size are lower than the data for 59 nm neck size and higher than those for smaller neck sizes,[23,24] as expected.

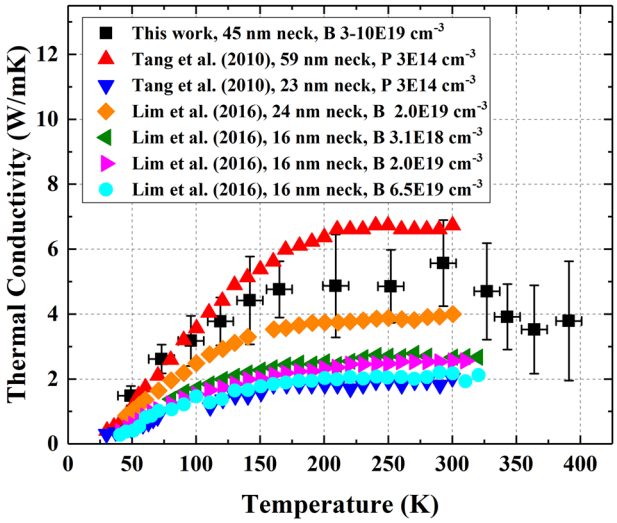

FIG. 5. Temperature dependence of the in-plane thermal conductivity of the holey Si thin film measured by heat diffusion imaging, compared with that of holey Si thin films with the same thickness (100 nm) but different neck sizes from the literature.[23,24] The carrier concentration of each sample is noted in the legend, with B for boron-doped and P for phosphorus doped.

IV. CONCLUSION

We have measured the in-plane thermal conductivity of holey Si and plain Si thin films from 40 K to 400 K using heat diffusion imaging, which combines thermoreflectance imaging with the heat spreader method. By comparing the obtained data for plain Si with values measured by in-plane TDTR and from the literature, we have demonstrated the reliability of our method. Heat diffusion imaging can be implemented to measure the thermal conductivity of supported thin films with minimum required micro-fabrication processes and is of great importance in the study of heat transport in thin films.

SUPPLEMENTARY MATERIAL

See the supplementary material for discussion on accuracy of in-plane TDTR measurement, determination of steady state and thermoreflectance signals from the substrate layers in heat diffusion imaging, SEM image of the holey Si structure, and example temperature decay curves under the 60× objective.

ACKNOWLEDGMENTS

This work was supported by the NSF under Grant No. 1653268 and was supported in part under a MURI program through the Office of Naval Research, Grant No. N00014-18-1-2429. D.H.O. is grateful for funding from the National Defense Science and Engineering Graduate (NDSEG) Fellowship. The authors would like to thank Professor J. E. Bowers for providing the thin film samples.

DATA AVAILABILITY

The data that support the findings of this study are available from the corresponding author upon reasonable request.

REFERENCES

[1]E. Pop, "Energy dissipation and transport in nanoscale devices," Nano Res. **3**, 147–169 (2010).
[2]J. S. Park, W.-J. Maeng, H.-S. Kim, and J.-S. Park, "Review of recent developments in amorphous oxide semiconductor thin-film transistor devices," Thin Solid Films **520**, 1679–1693 (2012).
[3]M. A. Green, "Thin-film solar cells: Review of materials, technologies and commercial status," J. Mater. Sci. **18**, 15–19 (2007).
[4]L. Martinu and D. Poitras, "Plasma deposition of optical films and coatings: A review," J. Vac. Sci. Technol., A **18**, 2619–2645 (2000).
[5]J.-S. Park, H. Chae, H. K. Chung, and S. I. Lee, "Thin film encapsulation for flexible AM-OLED: A review," Semicond. Sci. Technol. **26**, 034001 (2011).
[6]Y. C. Tai, C. H. Mastrangelo, and R. S. Muller, "Thermal conductivity of heavily doped low-pressure chemical vapor deposited polycrystalline silicon films," J. Appl. Phys. **63**, 1442–1447 (1988).
[7]M. Asheghi, K. Kurabayashi, R. Kasnavi, and K. E. Goodson, "Thermal conduction in doped single-crystal silicon films," J. Appl. Phys. **91**, 5079–5088 (2002).
[8]W. Liu and M. Asheghi, "Phonon-boundary scattering in ultrathin single-crystal silicon layers," Appl. Phys. Lett. **84**, 3819–3821 (2004).
[9]D. G. Cahill, "Thermal conductivity measurement from 30 to 750 K: the 3ω method," Rev. Sci. Instrum. **61**, 802–808 (1990).
[10]D. G. Cahill, "Analysis of heat flow in layered structures for time-domain thermoreflectance," Rev. Sci. Instrum. **75**, 5119–5122 (2004).
[11]Y. S. Ju, K. Kurabayashi, and K. E. Goodson, "Thermal characterization of anisotropic thin dielectric films using harmonic Joule heating," Thin Solid Films **339**, 160–164 (1999).
[12]K. Kurabayashi, M. Asheghi, M. Touzelbaev, and K. E. Goodson, "Measurement of the thermal conductivity anisotropy in polyimide films," J. Microelectromech. Syst. **8**, 180–191 (1999).
[13]W. Jang, Z. Chen, W. Bao, C. N. Lau, and C. Dames, "Thickness-dependent thermal conductivity of encased graphene and ultrathin graphite," Nano Lett. **10**, 3909–3913 (2010).
[14]C. Dames, "Measuring the thermal conductivity of thin films: 3 omega and related electrothermal methods," Annu. Rev. Heat Trans. **16**, 7–49 (2013).
[15]M. S. Aubain and P. R. Bandaru, "In-plane thermal conductivity determination through thermoreflectance analysis and measurements," J. Appl. Phys. **110**, 084313 (2011).
[16]Z. Bian, J. Christofferson, A. Shakouri, and P. Kozodoy, "High-power operation of electroabsorption modulators," Appl. Phys. Lett. **83**, 3605–3607 (2003).
[17]Y. Zhang, J. Christofferson, A. Shakouri, D. Li, A. Majumdar, Y. Wu, R. Fan, and P. Yang, "Characterization of heat transfer along a silicon nanowire using thermoreflectance technique," IEEE Trans. Nanotechnol. **5**, 67–74 (2006).
[18]T. Favaloro, A. Ziabari, J.-H. Bahk, P. Burke, H. Lu, J. Bowers, A. Gossard, Z. Bian, and A. Shakouri, "High temperature thermoreflectance imaging and transient Harman characterization of thermoelectric energy conversion devices," J. Appl. Phys. **116**, 034501 (2014).
[19]K. Maize, G. Pavlidis, E. Heller, L. Yates, D. Kendig, S. Graham, and A. Shakouri, "High resolution thermal characterization and simulation of power AlGaN/GaN HEMTs using micro-Raman thermography and 800 picosecond transient thermoreflectance imaging," in *2014 IEEE Compound Semiconductor Integrated Circuit Symposium (CSICS)* (IEEE, 2014), pp. 1–8.
[20]S. Nadri, C. M. Moore, N. D. Sauber, L. Xie, M. E. Cyberey, J. T. Gaskins, A. W. Lichtenberger, N. Scott Barker, P. E. Hopkins, M. Zebarjadi, and R. M. Weikle, "Thermal characterization of quasi-vertical GaAs Schottky diodes integrated on silicon," IEEE Trans. Electron Devices **66**, 349–356 (2019).
[21]J.-K. Yu, S. Mitrovic, D. Tham, J. Varghese, and J. R. Heath, "Reduction of thermal conductivity in phononic nanomesh structures," Nat. Nanotechnol. **5**, 718–721 (2010).

[22]Q. Hao, Y. Xiao, and H. Zhao, "Characteristic length of phonon transport within periodic nanoporous thin films and two-dimensional materials," J. Appl. Phys. **120**, 065101 (2016).
[23]J. Tang, H.-T. Wang, D. H. Lee, M. Fardy, Z. Huo, T. P. Russell, and P. Yang, "Holey silicon as an efficient thermoelectric material," Nano Lett. **10**, 4279–4283 (2010).
[24]J. Lim, H.-t. Wang, J. Tang, S. C. Andrews, H. So, J. Lee, D. H. Lee, T. P. Russell, and P. Yang, "Simultaneous thermoelectric property measurement and incoherent phonon transport in holey silicon," ACS Nano **10**, 124–132 (2016).
[25]M. Nomura, J. Shiomi, T. Shiga, and R. Anufriev, "Thermal phonon engineering by tailored nanostructures," Jpn. J. Appl. Phys. **57**, 080101 (2018).
[26]J. Christofferson and A. Shakouri, "Thermoreflectance based thermal microscope," Rev. Sci. Instrum. **76**, 024903 (2005).
[27]F. P. Incropera, D. P. DeWitt, T. L. Bergman, and A. S. Lavine, *Fundamentals of Heat and Mass Transfer*, 6th ed. (Wiley, Hoboken, NJ, 2007).
[28]M. Asheghi, M. N. Touzelbaev, K. E. Goodson, Y. K. Leung, and S. S. Wong, "Temperature-dependent thermal conductivity of single-crystal silicon layers in SOI substrates," J. Heat Transfer **120**, 30–36 (1998).
[29]K. Kang, Y. K. Koh, C. Chiritescu, X. Zheng, and D. G. Cahill, "Two-tint pump-probe measurements using a femtosecond laser oscillator and sharp-edged optical filters," Rev. Sci. Instrum. **79**, 114901 (2008).
[30]P. E. Hopkins, J. R. Serrano, L. M. Phinney, S. P. Kearney, T. W. Grasser, and C. T. Harris, "Criteria for cross-plane dominated thermal transport in multilayer thin film systems during modulated laser heating," J. Heat Transfer **132**, 081302 (2010).
[31]A. J. Schmidt, X. Chen, and G. Chen, "Pulse accumulation, radial heat conduction, and anisotropic thermal conductivity in pump-probe transient thermoreflectance," Rev. Sci. Instrum. **79**, 114902 (2008).
[32]P. Jiang, X. Qian, X. Gu, and R. Yang, "Probing anisotropic thermal conductivity of transition metal dichalcogenides MX 2 (M = Mo, W and X = S, Se) using time-domain thermoreflectance," Adv. Mater. **29**, 1701068 (2017).
[33]*CRC Handbook of Chemistry and Physics*, edited by D. R. Lide (CRC Press LLC, 2005).
[34]R. B. Wilson and D. G. Cahill, "Anisotropic failure of Fourier theory in time-domain thermoreflectance experiments," Nat. Commun. **5**, 5075 (2014).
[35]T. Favaloro, J.-H. Bahk, and A. Shakouri, "Characterization of the temperature dependence of the thermoreflectance coefficient for conductive thin films," Rev. Sci. Instrum. **86**, 024903 (2015).
[36]Y. S. Touloukian, R. W. Powell, C. Y. Ho, and P. G. Klemens, *Thermal Conductivity: Nonmetallic Solids*, Thermophysical Properties of Matter Vol. 2 (IFI/Plenum, New York, 1970).
[37]S. S. Mahajan, G. Subbarayan, and B. G. Sammakia, "Estimating kapitza resistance between Si-SiO_2 interface using molecular dynamics simulations," IEEE Trans. Compon., Packag., Manuf. Technol. **1**, 1132–1139 (2011).
[38]J. Chen, G. Zhang, and B. Li, "Thermal contact resistance across nanoscale silicon dioxide and silicon interface," J. Appl. Phys. **112**, 064319 (2012).
[39]E. Lampin, Q.-H. Nguyen, P. A. Francioso, and F. Cleri, "Thermal boundary resistance at silicon-silica interfaces by molecular dynamics simulations," Appl. Phys. Lett. **100**, 131906 (2012).
[40]W. Liu and M. Asheghi, "Thermal conductivity measurements of ultra-thin single crystal silicon layers," J. Heat Transfer **128**, 75–83 (2006).